3074 *Biochemistry* **2010,** *49,* 3074–3082
DOI: 10.1021/bi1002647

BIOCHEMISTRY
including biophysical chemistry & molecular biology
Article

Orientations of Carboxylate Groups Coupled to the Mn Cluster in the Photosynthetic Oxygen-Evolving Center As Studied by Polarized ATR-FTIR Spectroscopy[†]

Mitsuhiro Iizasa, Hiroyuki Suzuki, and Takumi Noguchi*

Institute of Materials Science, University of Tsukuba, Tsukuba, Ibaraki 305-8573, Japan

Received February 22, 2010; Revised Manuscript Received March 14, 2010

ABSTRACT: It is essential to clarify the structures and interactions of amino acids surrounding the Mn cluster in photosystem II (PSII) to understand the molecular mechanism of photosynthetic oxygen evolution. In this study, polarized attenuated total reflection Fourier transform infrared spectroscopy (ATR-FTIR) was applied for the first time to PSII to investigate the orientation of carboxylate groups coupled to the oxygen-evolving Mn cluster. PSII membranes from spinach were oriented on the surface of a silicon ATR crystal, and flash-induced polarized ATR-FTIR difference spectra for the $S_1 \rightarrow S_2$ transition (S_2/S_1 spectra) were obtained. The distribution of membrane orientations by mosaic spread was estimated from the semiquinone CO peak in polarized Q_A^-/Q_A difference spectra recorded using the same oriented sample by buffer exchange. The orientations of carboxylate groups coupled to the Mn cluster were estimated from the dichroic ratios of the symmetric COO^- bands in the polarized S_2/S_1 ATR-FTIR spectra. We found that most of the carboxylate groups perturbed during the $S_1 \rightarrow S_2$ transition, due to direct ligation to the Mn cluster or though a hydrogen bond network, have orientations in a relatively narrow angle range of 34−48° with respect to the membrane normal. Implications of the obtained orientations and the changes upon formation of S_2 are discussed on the basis of the information from previous FTIR studies and the X-ray structures. The results in this study show that polarized ATR-FTIR difference spectroscopy is a fruitful method for investigating the orientations and their reaction-induced changes in redox cofactors and coupled amino acid side chains in photosynthetic proteins.

Atmospheric oxygen that is essential for almost all lives on Earth basically relies on photosynthetic oxygen evolution performed by plants and cyanobacteria. The oxygen-evolving reaction, that is, oxidation of water to produce molecular oxygen utilizing solar energy, takes place in photosystem II (PSII)[1] protein complexes embedded in thylakoid membranes (*1*−*4*). The catalytic site of oxygen evolution in PSII is the oxygen-evolving center (OEC), which consists of a metal cluster core of four Mn atoms and one Ca atom called the Mn cluster and surrounding amino acid ligands from the D1 and CP43 subunits. In PSII, light-induced charge separation takes place at the monomeric chlorophyll Chl_{D1} to form a radical pair between the chlorophyll dimer P_{680} and the pheophytin electron acceptor $Pheo_{D1}$, $P_{680}^+Pheo_{D1}^-$ (*5*). On the electron acceptor side, an electron is transferred from $Pheo_{D1}^-$ to the primary quinone electron acceptor Q_A and then to the secondary quinone electron acceptor Q_B, while on the electron donor side, P_{680}^+ abstracts an electron from the OEC through the Tyr electron donor Y_Z (D1-Tyr161). In the OEC, two water molecules are converted into one molecular oxygen and four protons through a light-driven cycle of five intermediates called S_i states (i = 0−4) (*1*−*4*). When successive flashes are applied, each flash advances the S_i state to the S_{i+1} state (i = 0−3), and the transient S_4 state relaxes to the S_0 state, releasing molecular oxygen. Since the S_1 state is the most stable in the dark, oxygen is evolved after the first three flashes and then every four flashes.

Recent X-ray diffraction (XRD) studies of the PSII core complexes from thermophilic cyanobacteria have provided the PSII structures at 2.9−3.7 Å resolution (*6*−*9*) and predicted the positions of the Mn and Ca atoms and of amino acid ligands: six carboxylate groups from D1-Asp170, D1-Glu189, D1- Glu333, D1-Asp342, D1-Ala344 (C-terminus), and CP43-Glu354 and one imidazole from D1-His332. However, these models of the Mn cluster and the amino acid ligation pattern are significantly different from each other except for the basic structure with the trimer/monomer arrangement of the Mn_4 core, which has previously been proposed by EPR analyses (*10*, *11*), and the Ca atom coupled with the trimer part. This discrepancy is due partly to the limited resolutions (2.9−3.7 Å) available so far, which are not enough to resolve the atomic-level structure. In addition, it was shown by XANES and EXAFS studies that the X-ray dose used to collect the XRD data reduced the Mn(III) and Mn(IV) ions to Mn(II), which distorted the structure of the Mn cluster (*12*, *13*). Indeed, Yano et al. (*14*) showed that none of four possible Mn_4Ca cluster models obtained by polarized EXAFS agree with the models obtained from XRD studies. They placed their Mn_4Ca cluster models into the protein structure obtained by the XRD study (*7*), providing OEC models with different amino acid ligation patterns. These models, however, resulted in

[†]This study was supported by Grants-in-Aid for Scientific Research from the Ministry of Education, Culture, Sports, Science and Technology (21108506, 21370063, and 17GS0314).

*To whom correspondence should be addressed. Phone: +81-29-853-5126. Fax: +81-29-853-4490. E-mail: tnoguchi@ims.tsukuba.ac.jp.

[1]Abbreviations: ATR, attenuated total reflection; DCMU, 3-(3,4-dichlorophenyl)-1,1-dimethylurea; DFT, density functional theory; EPR, electron paramagnetic resonance; EXAFS, extended X-ray absorption fine structure; FTIR, Fourier transform infrared; IR, infrared; IRE, internal reflection element; Mes, 2-(*N*-morpholino)ethanesulfonic acid; OEC, oxygen-evolving center; P680, special pair chlorophyll of photosystem II; PMS, phenazine methosulfate; PQ-1, plastoquinone-1; PSII, photosystem II; Q_A, primary quinone electron acceptor; Q_B, secondary quinone electron acceptor; XANES, X-ray absorption near-edge structure; XRD, X-ray diffraction.

 Published on Web 03/16/2010

unsatisfactory metal−ligand distances, which were explained by modification of the ligand positions by X-ray damage to the Mn cluster (*14*). Further analyses using the XRD and EXAFS data, including repositioning of amino acid ligands (*15*, *16*) and optimization by density functional theory (DFT) calculations (*17*−*19*), also proposed different OEC models with different ligation patterns. Thus, in spite of recent extensive XRD and EXAFS investigations, the structure of OEC has not yet been determined.

Information about the structure of the OEC has also been obtained by Fourier transform infrared (FTIR) spectroscopy, which is a powerful method for studying the structures and reactions of amino acid residues coupled to the redox cofactors in photosynthetic proteins (*20*, *21*). Light-induced FTIR difference spectra of the OEC (*22*−*25*) have been obtained during S-state transitions, showing that several carboxylate groups are involved in the ligands to the Mn cluster and the reactions in the OEC (*26*−*28*). Among them, FTIR bands of the C-terminus (D1-Ala344) (*25*, *29*−*31*) and CP43-Glu354 (*32*, *33*) have been detected by site-directed mutations and/or selective isotope labeling, strongly suggesting ligation of these residues to Mn ions. An imidazole band, probably from D1-His332 or D1-His337, was also detected by selective isotope labeling of imidazole groups, indicative of coordination to a Mn ion (*34*, *35*). The His coordination is in agreement with the previous ESEEM study (*36*).

In this study, we have for the first time applied the polarized attenuated total reflection (ATR) FTIR spectroscopy to photosynthetic proteins to study the orientations of amino acid side chains coupled to the Mn cluster. This method is useful for studying the orientations of the transition dipole moments of normal mode vibrations in membrane proteins adsorbed to the surface of an internal reflection element (IRE) (*37*). So far, ATR-FTIR has mostly been used to examine the orientations of the main chains of polypeptides or proteins in lipid bilayers (*38*−*41*). By combination of light-induced FTIR difference spectroscopy, spectra of different redox cofactors can be obtained for the same sample adsorbed on the IRE surface by buffer exchange (*42*, *43*). Analysis of polarized ATR-FTIR difference spectra upon the $S_1 \rightarrow S_2$ transition, along with the estimation of a distribution of membrane orientations using a Q_A^- signal, provided information about the orientations of carboxylate groups coupled to the Mn cluster in the S_1 and S_2 states.

MATERIALS AND METHODS

Sample Preparation for ATR-FTIR Measurements. Oxygen-evolving PSII membranes were prepared from spinach as reported previously (*44*) and suspended in Mes buffer [buffer A: 40 mM Mes-NaOH, 20 mM NaCl, and 20 mM $CaCl_2$ (pH 6.5)]. Sample preparation for ATR-FTIR measurements was followed by the method described previously (*43*). Briefly, an aliquot of the PSII sample (5 μL, 1 mg of Chl/mL) washed with distilled water by centrifugation was loaded on the surface of a three-reflection silicon prism (3 mm in diameter) of the ATR accessory (DuraSampl*IR* II, Smiths Detection) and dried under a nitrogen gas flow. Subsequently, a flow cell consisting of a transparent acrylic plate and a rubber spacer was attached to the sample stage, and buffer A was allowed to flow into the cell (Figure 1A). A sufficient thickness of the sample to cover the penetration depth of the IR beam (< 1 μm at 1650 cm^{-1}) was confirmed by monitoring the ATR-FTIR absorption while changing the amount of sample loaded. The temperature of the silicon surface was maintained at 10 °C by circulation of cooled water through a copper plate attached to the sample stage.

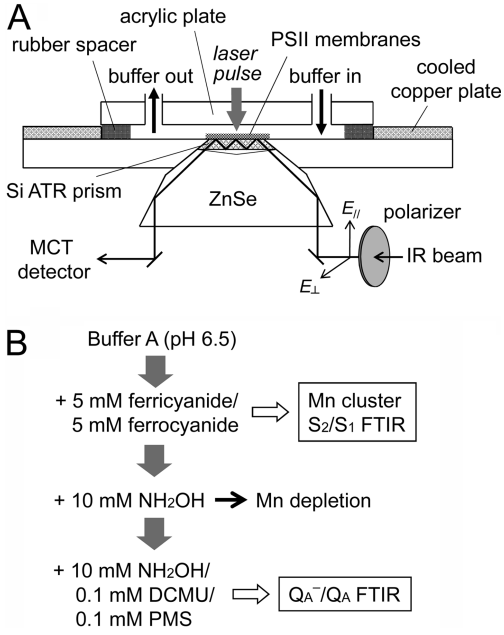

FIGURE 1: (A) Schematic diagram of the ATR cell used for light-induced polarized ATR-FTIR difference measurements and (B) procedure for the measurements of S_2/S_1 and Q_A^-/Q_A ATR-FTIR difference spectra using the same oriented sample of PSII membranes by exchanging buffers.

Polarized ATR-FTIR Measurements. FTIR spectra were recorded on a Bruker IFS-66/S spectrophotometer equipped with an MCT detector (InfraRed D313-L). All spectra were recorded at 4 cm^{-1} resolution. Illumination was performed with a flash of light from a Q-switched Nd:YAG laser (Quanta-Ray GCR-130; 532 nm, ~7 ns fwhm, ~9 mJ cm^{-2} $pulse^{-1}$ at the sample). Polarized ATR-FTIR difference spectra were recorded with perpendicular or parallel polarization of the incident IR beam using a wire grid polarizer (ST-Japan STJ-1001). For the measurement of S_2/S_1 FTIR difference spectra, buffer A in the sample cell was replaced with buffer A containing 5 mM potassium ferricyanide and 5 mM potassium ferrocyanide[2] (Figure 1B). Single-beam spectra with 20 s scans (40 scans) were recorded twice before and once after single-flash illumination, and dark-minus-dark (representing noise levels) and light-minus-dark difference spectra were calculated. This measurement was repeated with intervals of 5 min for dark relaxation. The polarizations of the incident IR beam were changed every five measurements, and spectra of 80 measurements in total for each polarization were averaged.

After the measurement of the S_2/S_1 difference spectra, Q_A^-/Q_A difference spectra were recorded using the same oriented sample by exchanging buffers (*43*) to evaluate the disorder in membrane orientation. The Mn cluster was first removed by incubation in buffer A containing 10 mM NH_2OH for 30 min, and then it was replaced with buffer A containing 10 mM NH_2OH, 0.1 mM

[2]Ferrocyanide is included in the buffer to decrease the redox potential for avoiding preoxidation of the non-heme iron by ferricyanide. In the previous S_2/S_1 measurements (*26*), a ferrocyanide:ferricyanide ratio of 9:1 was used because the sample was subjected to long dark adaptation. In our experiment, however, measurements were repeated with 5 min dark intervals, and thus, a lower ratio of 1:1 was sufficient to delay the reoxidation of the non-heme iron and remove its signals from the FTIR spectra.

DCMU, and 0.1 mM PMS. PMS works as an electron acceptor when Q_A^- is relaxed in the dark in repetitive measurements. A set of two 40 s measurements before single-flash illumination and one 40 s measurement after illumination was repeated with 12 min dark intervals. The polarizations of the IR beam were changed every five measurements, and spectra of 40 measurements in total for each polarization were averaged. Two sets of experiments using two samples were performed, and the spectra were averaged for the final data.

Data Analysis. The dichroic ratio R was defined as $\Delta A_{\parallel}/\Delta A_{\perp}$, in which $\Delta A_{\parallel}$ and $\Delta A_{\perp}$ are absorbance changes measured with parallel and perpendicular polarizations, respectively. In ATR-FTIR measurement, R is related to an orientational order parameter S (*37*)

$$R = \frac{A_{\parallel}}{A_{\perp}} = \frac{E_x^2}{E_y^2} + \frac{E_z^2}{E_y^2}\left(1 + \frac{3S}{1-S}\right) \quad (1)$$

where E_x^2, E_y^2, and E_z^2 are the time-averaged square electric field amplitudes of the evanescent wave:

$$E_x^2 = \frac{4\cos^2\theta(\sin^2\theta - n_{21}^2)}{(1-n_{21}^2)[(1+n_{21}^2)\sin^2\theta - n_{21}^2]} \quad (2)$$

$$E_y^2 = \frac{4\cos^2\theta}{1-n_{21}^2} \quad (3)$$

$$E_z^2 = \frac{4\cos^2\theta \times \sin^2\theta}{(1-n_{21}^2)[(1+n_{21}^2)\sin^2\theta - n_{21}^2]} \quad (4)$$

where n_{21} is the ratio of the refractive index of the external medium, n_2, to that of the IRE, n_1 ($n_{21} = n_2/n_1$), and θ is the angle of the incident IR beam with respect to the normal of the IRE surface. For PSII membranes as a sample, the n_1 value of 1.5, which was previously estimated for chloroplasts (*45*, *46*), was adopted. When $n_2 = 3.42$ for the Si crystal as the IRE and $\theta = 45°$, $E_x^2 = 1.887$, $E_y^2 = 2.476$, and $E_z^2 = 3.066$.

The experimental order parameter S obtained from R by eq 1 is expressed as

$$S = S_{ms}S_{dp} \quad (5)$$

where S_{ms} represents a distribution of the membrane normals with respect to the normal of the IRE surface by the mosaic spread (*45*, *46*) and S_{dp} is an order parameter representing the orientation of the transition dipole moment of a normal mode vibration. If the membranes are perfectly oriented, $S_{ms} = 1$, whereas a totally random orientation gives an S_{ms} of 0. In the latter case, $R = 2$ in ATR-FTIR because of a two times larger penetration depth for parallel polarization compared with perpendicular polarization, in contrast to an R of 1 in transmission IR spectroscopy. S_{dp} is related to the angle of the transition dipole with respect to the membrane normal, φ, with the equation

$$S_{dp} = \frac{3\cos^2\varphi - 1}{2} \quad (6)$$

Thus, once S_{ms} is determined for the membrane sample, φ of a concerned vibration can be evaluated from the experimental value of R using eqs 1, 5, and 6.

DFT Calculations. Density functional theory (DFT) calculations were performed using the Gaussian03 program package (*47*). The B3LYP functional (*48*, *49*) with the 6-31+G(d) basis set was used to optimize the geometry of a hydrogen-bonded complex of plastoquinone-1 (PQ-1) (*50*), a model of Q_A^-, and calculate the transition dipole moments of the normal mode vibrations.

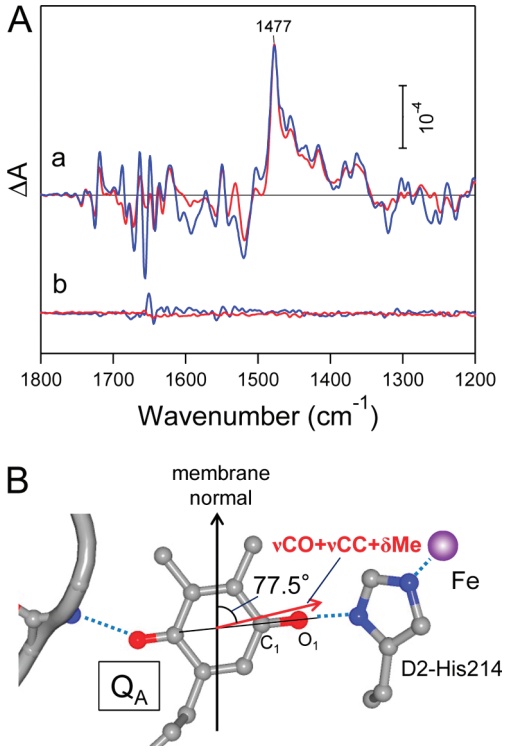

FIGURE 2: (A) Polarized ATR-FTIR difference spectra upon light-induced Q_A^- formation of oriented PSII membranes (a) and the corresponding dark-minus-dark difference spectra representing noise levels (b). Spectra were recorded with parallel (blue lines) and perpendicular (red lines) polarizations of the incident IR light. The zero line is shown as a thin black line in part a. (B) Orientation of the transition dipole moment of the CO stretching vibration of the Q_A^- semiquinone anion with respect to the C_2 axis of the PSII core dimer. The orientation of Q_A was taken from the X-ray structure of Guskov et al. (*8*), and the deviation of the transition dipole moment from the direction of the $C_1{-}O_1$ bond was estimated by DFT calculation of a model PQ-1^- complex hydrogen bonded with water at each CO group (Figure S1 of the Supporting Information) (*50*).

RESULTS

Estimation of S_{ms} Using Polarized Q_A^-/Q_A ATR-FTIR Difference Spectra. The order parameter for a distribution of membrane orientations by the mosaic spread, S_{ms}, was estimated using the CO stretching band of Q_A^-. The polarized Q_A^-/Q_A ATR-FTIR difference spectra of the PSII membranes oriented on the Si IRE surface are presented in Figure 2Aa (blue and red lines represent parallel and perpendicular polarizations, respectively). The zero line is also shown as a thin black line. These spectra were obtained after the measurements of the S_2/S_1 difference spectra (see below) without changing the sample by in situ buffer exchange (Figure 1B) (*43*), and hence, the S_{ms} obtained from the Q_A^-/Q_A spectra can be directly used in the analysis of the S_2/S_1 spectra. If the membranes are randomly oriented, the spectrum from a parallel polarization (blue line) should show a 2 times greater intensity than that from a perpendicular polarization (red line) ($R = 2$). However, the two spectra in the 1500−1350 cm^{-1} region exhibited similar intensities, while the spectra in the 1750−1550 cm^{-1} region exhibited different dichroic ratios depending on the peaks,

indicating that the PSII membranes are highly oriented. The dichroic ratio R at the prominent positive peak at 1477 cm^{-1}, which has been assigned to the asymmetric CO stretching vibration of Q_A^- (*50*, *51*), was estimated to be 0.99 ± 0.01. The error was estimated by taking into account the noise levels (root-mean-square values in the 1490−1470 cm^{-1} region) revealed in the dark-minus-dark difference spectra obtained before flash illumination (Figure 2Ab).

We previously performed vibrational analysis of the semiquinone anion using PQ-1 with each CO group hydrogen bonded with a water molecule, as a model of Q_A^- having symmetric hydrogen bonding interactions, by DFT calculations at the B3LYP/6-31+G(d) level (*50*). The obtained band pattern reproduced well the Q_A^- FTIR spectra measured in the presence of DCMU as a herbicide. The CO vibration responsible for the intense 1477 cm^{-1} peak is strongly coupled with the ring CC stretches and the methyl deformations (*50*), and hence, the direction of the transition dipole moment is predicted to be slightly deviated from that of the CO bonds. Using the optimized geometries obtained in the latter study, we now calculated the direction of the transition dipole moment of the IR-active CO stretching mode. It was shown that the direction of the transition dipole of this vibration deviates from that of the C_1−O_1 bond by 7° to the side of the methyl group on the ring plane (Figure S1 of the Supporting Information). We note that a similar deviation of 6° was estimated using a free PQ-1 anion as a model, and thus, the transition dipole of this vibration is not very sensitive to the hydrogen bond form.

Using the atomic coordinates from the X-ray structure at 2.9 Å resolution of Guskov et al. (PDB entry 3BZ1) (*8*), the orientation of the C_1−O_1 bond of Q_A with respect to the C_2 axis of the PSII core dimer was estimated to be 84°. By combining this result with the result of the DFT calculation described above, we estimated the orientation of the transition dipole moment of the CO stretching vibration of Q_A^- with respect to the membrane normal to be 77°. From eqs 1, 5, and 6 using an R of 0.99 ± 0.01 and a φ of 77°, S_{ms} was estimated to be 0.87 ± 0.01, confirming that the PSII membranes used for the ATR-FTIR measurements are highly oriented on the Si surface. The accuracy of the obtained S_{ms} depends on that of the Q_A orientation in the X-ray structure. The X-ray structures of Loll et al. (3.0 Å resolution) (*7*), Ferreira et al. (3.5 Å resolution) (*6*), and Kawakami et al. (3.7 Å resolution) (*9*) provide C_1−O_1 orientations of 89°, 85°, and 77°, respectively, with respect to the membrane normal. The S_{ms} values estimated using these three X-ray structures taking into account the DFT result are 0.78, 0.75, and 1.1, respectively, the last of which is an unrealistic value. These estimations indicate that the S_{ms} of the PSII membranes is at least higher than 0.75 and most likely around 0.9.

Polarized S_2/S_1 ATR-FTIR Difference Spectra. The polarized S_2/S_1 ATR-FTIR difference spectra of the oriented PSII membranes are presented in Figure 3a (blue and red lines for parallel and perpendicular polarizations, respectively). The noise levels are revealed as dark-minus-dark difference spectra in Figure 3b. The overall features of the polarized S_2/S_1 spectra are very similar to those of the previous S_2/S_1 spectra measured using the transmission (*26*) and ATR (*43*) methods. Bands in the 1450−1300 cm^{-1} region represent the symmetric COO^- stretching vibrations of carboxylate groups most likely from the direct ligands to the Mn cluster, while the 1600−1450 cm^{-1} region is due to the overlap of asymmetric COO^- bands and amide II bands (NH bend and CN stretch of backbone amides) (*24*, *25*, *27*, *28*). Bands

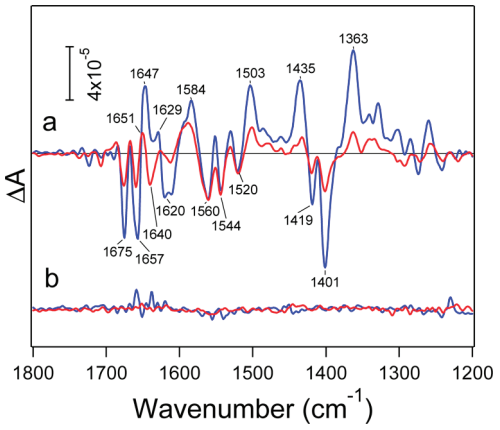

FIGURE 3: Polarized ATR-FTIR difference spectra upon the light-induced $S_1 \rightarrow S_2$ transition of oriented PSII membranes (a) and the corresponding dark-minus-dark difference spectra representing noise levels (b). Spectra were measured with parallel (blue lines) and perpendicular (red lines) polarizations of the incident IR light. The zero line is shown as a thin black line in part a.

in the 1700−1600 cm^{-1} region mostly arise from the amide I vibrations (C═O stretch of backbone amides). It is notable that the dichroic ratios of the major bands in the symmetric COO^- region (e.g., bands at 1435, 1419, 1401, and 1363 cm^{-1}) are all large, whereas those in the 1600−1450 cm^{-1} region (e.g., bands at 1584, 1560, 1544, and 1520 cm^{-1}) are relatively small except for the positive band at 1503 cm^{-1}. Although the dichroic ratios in the amide I region (1700−1600 cm^{-1}) are relatively large, the peak positions in the 1600−1650 cm^{-1} region do not agree between the parallel and perpendicular polarizations, indicating a severe overlap of bands representing different orientations. The latter observation is consistent with the X-ray structures (*6*−*9*) showing that the Mn cluster is surrounded by polypeptide chains with loop or α-helical conformations oriented in different directions.

The direction of the transition dipole moment of the symmetric COO^- stretching vibration basically agrees with the orientation of the COO^- group, which is represented by the direction of the C−C bond in the $CCOO^-$ unit of Asp and Glu and the C-terminus (Figure 4B). Also, other vibrations of PSII proteins interfere only slightly with the symmetric COO^- region (1450−1300 cm^{-1}) in the S_2/S_1 spectrum (*27*). Thus, this region is appropriate for detailed analysis for the investigation of the orientations of the carboxylate groups coupled to the Mn cluster. In contrast, the asymmetric COO^- region is not suitable for analysis because of a severe overlap with amide II bands (*27*, *28*) and the direction of the transition dipole that does not directly match that of the COO^- group.

Figure 4A shows the expanded view of the symmetric COO^- region of the polarized S_2/S_1 ATR-FTIR difference spectra. Parallel (blue line) and perpendicular (red line) spectra exhibit very similar features, although the overall intensity is much lower in the latter spectrum. In both polarizations, peak positions were virtually identical in major peaks except that the peaks at 1435 and 1329 cm^{-1} in the parallel polarization shift to 1433 and 1334 cm^{-1}, respectively, in the perpendicular polarization.

Table 1 summarizes the dichroic ratios (R) and the angles (φ) of the transition dipole moments with respect to the membrane normal, estimated using an S_{ms} of 0.87 ± 0.01, at 1435, 1419, 1401, and 1363 cm^{-1}, the frequencies showing major peaks in the parallel polarization. The R and φ values at 1433, 1393, and 1340 cm^{-1},

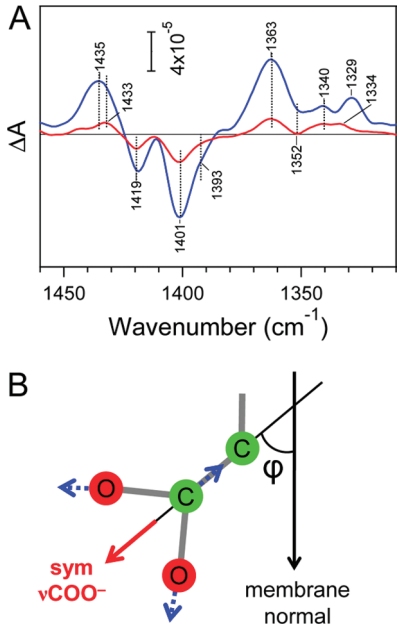

FIGURE 4: (A) Expanded spectra in the symmetric COO^- stretching region of the polarized ATR-FTIR difference spectra of the $S_1 \rightarrow S_2$ transition measured with parallel (blue lines) and perpendicular (red lines) polarizations. The zero line is shown as a thin black line. (B) Orientation of the transition moment of the symmetric stretching vibration of a carboxylate group, assuming it has a symmetric structure.

where CP43-Glu354 or the C-terminus is expected to provide a large contribution (see below for a detailed discussion of the assignments of these carboxylate groups), are also included. Reflecting the relatively large R values in the overall symmetric COO^- region, the estimated angles of transition dipole moments provide relatively small values ranging between 34° and 48°. Errors of angles, which were estimated taking into consideration the noise levels of the spectra (Figure 3b) and the errors of S_{ms} (0.87 ± 0.01), range from 2° and 5°. It is noted that the effect of inaccuracy of the Q_A orientation depending on the X-ray structures was similar to or smaller than this error range; for example, if the S_{ms} value of 0.75−1.0 is used for the calculation of φ at 1401 cm^{-1}, the resultant φ ranges between 44° and 47°, which is similar to the value of 45 ± 2° obtained with an S_{ms} of 0.87.

DISCUSSION

In this study, we have for the first time applied polarized ATR-FTIR spectroscopy to photosynthetic membrane proteins to determine the orientations of carboxylate groups coupled to the Mn cluster in PSII. The benefits of the polarized ATR-FTIR method over the conventional transmission method are twofold. First, using the ATR method, the spectra of different cofactors can be obtained using the same sample attached to the IRE surface by exchanging buffers (*43*). This is advantageous in determining the S_{ms} of the oriented membranes using the polarized spectra of a cofactor with a known orientation. Second, better orientations of the membranes can be obtained near the IRE surface, where the ATR-FTIR spectra of a sample are selectively measured.

We first estimated the distribution of the membrane orientations using the dichroic ratio R of the CO stretching band at 1477 cm^{-1} of Q_A^- in the Q_A^-/Q_A difference spectra (Figure 2A), which were obtained after the S_2/S_1 measurements using the same sample adsorbed to the Si surface. The S_{ms} was estimated to be 0.87 ± 0.01 from an R of 0.99 ± 0.01 using the orientation information of Q_A from the X-ray structure (*8*) and the direction of the transition dipole moment of the CO stretching mode, which is coupled with the CC stretches and methyl deformations, estimated by DFT calculations of a PQ-1 radical anion as a model of Q_A^- (Figure S1 of the Supporting Information). This value represents a mosaic spread of 17 ± 1°, which is consistent with or better than the previous reports (15−20° in ref *52* and 35−38° in ref *53*) for oriented PSII membranes assessed by the Y_D and cytochrome b_{559} EPR signals in polarized EXAFS studies. Thus, the PSII membranes used for the S_2/S_1 measurements were highly oriented on the Si surface.

The polarized S_2/S_1 ATR-FTIR difference spectra in the symmetric COO^- region showed that parallel and perpendicular spectra have very similar features, with a lower intensity in the latter spectrum, indicative of a relatively narrow range of R [R = 2.7−5.2 (Table 1)] at least for the major peaks. This observation indicates that the transition dipole moments of the symmetric COO^- vibrations affected by the $S_1 \rightarrow S_2$ transition have rather similar orientations. In fact, the estimated angles with respect to the membrane normal range between 34° and 48° at the prominent peaks at 1363, 1401, 1419, and 1435 cm^{-1} (Table 1). Since the direction of the transition dipole moment of the symmetric COO^- vibration virtually agrees with that of a COO^- group (Figure 4B) at least in a chelating or symmetric bridging bidentate coordination (*54*), this observation indicates that the carboxylate groups strongly coupled to the Mn cluster and their structures are perturbed during the $S_1 \rightarrow S_2$ transition mostly have orientations in a relatively narrow angle range of 34−48° with respect to the membrane normal.

Since the assignments of individual symmetric COO^- bands in the S_2/S_1 FTIR spectrum to specific amino acid residues are not yet well established (*24*, *25*), it is not easy to definitively correlate the angle information from the COO^- bands with the orientations of the carboxylate groups coupled to the Mn cluster. In the following, however, we will attempt to provide some discussion about the orientations and their changes of the specific carboxylate groups around the Mn cluster based on the information from the band assignments and the coordination changes of carboxylate groups from previous FTIR studies. The orientation information for the carboxylate groups in the S_1 state (or more reduced states by X-ray radiation) from the XRD studies is also taken into consideration. Note that although this discussion will focus on the carboxylate groups that are putative ligands to the Mn ions or those in the vicinity of the Mn cluster, there is also a possibility that carboxylate groups rather distant from the Mn cluster, but structurally coupled with it, are responsible for some of the symmetric COO^- bands in the FTIR spectra.

Table 2 compares the orientations of seven carboxylate groups around the Mn cluster (Figure 2B) with respect to the C_2 axis of the PSII core dimer obtained from the X-ray structures at 2.9−3.7 Å resolution. Among these carboxylate groups, D1-Asp170, D1-Glu189, D1-Glu333, D1-Asp342, D1-Ala344 (C-terminus), and CP43-Glu354 are the putative carboxylate ligands, while D1-Asp61 may not be a direct ligand. Note that the structure of Guskov et al. (*8*) (2.9 Å) was obtained by reprocessing the same XRD data used for the structure by Loll et al. (*7*) (3.0 Å). The angle of each carboxylate group is rather different from one X-ray structure to another; the maximum differences are 13°, 21°, 31°, 31°, 47°, 8°, and 22° for Asp61, Asp170, Glu189, Glu333, Asp342,

Table 1: Orientations of the Transition Dipole Moments of the Symmetric COO^- Stretching Vibrations Coupled to the Mn Cluster Estimated from the S_2/S_1 Polarized ATR-FTIR Difference Spectra

frequency (cm^{-1})	S state	dichroic ratio[a] R	angle[b] φ (deg)	note
1340	S_2	2.7 ± 0.5	47 ± 4	contribution of the C-terminus (D1-Ala344) ((*29*)−(*30*)(*31*))
1363	S_2	4.8 ± 0.6	35 ± 3	sensitive to Ca^{2+} depletion (*26*) and NH_3 treatment (*56*)
1393	S_1	2.9 ± 0.6	46 ± 5	contribution of CP43-Glu354 (*33*)
1401	S_1	3.0 ± 0.2	45 ± 2	sensitive to Ca^{2+} depletion (*26*)
1419	S_1	2.7 ± 0.4	48 ± 3	
1433	S_2	4.3 ± 0.6	38 ± 3	contribution of CP43-Glu354 (*33*)
1435	S_2	5.2 ± 0.9	34 ± 4	

[a]Errors were estimated from the noise levels of the spectra [rms value in the 1500−1300 cm^{-1} region of the dark-minus-dark spectra (Figure 3b)]. [b]Angles of the transition dipole moments with respect to the membrane normal were estimated from R using an S_{ms} of 0.87 ± 0.01.

Table 2: Orientations of the Carboxylate Groups around the Mn Cluster in the X-ray Structures

		angle (deg)[a]						
X-ray structure (PDB entry)	resolution (Å)	Asp61	Asp170	Glu189	Glu333	Asp342	Ala344[b]	Glu354[c]
Guskov et al. (3BZ1) (*8*)	2.9	55	38	73	63	59	76	49
Loll et al. (2AXT) (*7*)	3.0	60	17	78	43	56	75	50
Ferreira et al. (1S5L) (*6*)	3.5	47	26	47	66	15	73	50
Kawakami et al. (3A0B) (*9*)	3.7	54	23	60	74	62	81	71

[a]Angles of the C−C bond of the $CCOO^-$ unit with respect to the C_2 axis of the PSII dimer. [b]C-Terminus of the D1 subunit. [c]CP43-Glu354. Other residues are all on the D1 subunit.

Ala344, and CP43-Glu354, respectively. Even in the results of Guskov et al. (*8*) and Loll et al. (*7*), the orientations of Asp170 (17° vs 38°) and Glu333 (43° vs 63°) are significantly different. The relatively large discrepancies in the orientations of the carboxylate ligands in comparison with the discrepancy in the Q_A orientation (difference of 17° at most) indicate that the OEC indeed suffered from X-ray damage (*12*, *13*) and its X-ray structure is temporal. This was also asserted by the inconsistency of the core structure of the Mn cluster obtained by polarized EXAFS with that in the X-ray structures (*14*).

The assignment of the FTIR bands of CP43-Glu354 has been investigated using the CP43-Glu354Gln mutant of *Synechocystis* sp. PCC6803 by two groups. Strickler et al. (*32*) first measured an S_2/S_1 difference spectrum of this mutant and tentatively assigned the 1362/1378 cm^{-1} peaks in the wild type-minus-mutant double difference spectrum to symmetric COO^- vibrations of CP43-Glu354 in the S_2 and S_1 states. However, the corresponding spectrum by Shimada et al. (*33*) did not show a prominent band at 1362 cm^{-1} and instead showed a strong band at 1431 cm^{-1}, where a similar band was also observed at 1429 cm^{-1} in the spectrum of Strickler et al. (*32*). The band corresponding to the 1378 cm^{-1} band of Strickler et al. was detected at 1394 cm^{-1}. Thus, Shimada et al. (*33*) proposed that the symmetric COO^- bands of CP43-Glu354 are located at 1431 and 1393 cm^{-1} in the S_2 and S_1 states, respectively. Reasons for the differences between the spectra from two groups (*32*, *33*) are unknown at present. From these results, we tentatively assign the positive peak at 1433 cm^{-1} characteristic of perpendicular polarization and the negative shoulder at 1393 cm^{-1} in the polarized S_2/S_1 difference spectra of spinach PSII membranes (Figure 4A) to the signals that have a large contribution from CP43-Glu354.

The negative shoulder at 1393 cm^{-1} (Figure 4A) showed an angle of $46 \pm 5°$ (Table 1). Although a severe overlap with a large band at 1401 cm^{-1} hampers accurate estimation of the orientation of CP43-Glu354, this value agrees with the orientations of CP43-Glu354 in the X-ray structures at resolutions higher than 3.5 Å, 49−50° (Table 2), in the error range. In the S_2 state, the orientation of CP43-Glu354 can be estimated to be $38 \pm 3°$ (Table 1) from the dichroic ratio at 1433 cm^{-1} (Figure 4A, red line). The orientation change of ~8° upon formation of the S_2 state is consistent with the change from bridging to chelating coordination previously proposed from the decrease in the frequency gap between the asymmetric and symmetric COO^- vibrations (*33*). For a more accurate estimation of the CP43-Glu354 orientation avoiding severe overlap of bands, further polarized FTIR measurements are necessary for the isolated CP43-Glu354 bands in double difference spectra between the wild type and CP43-Glu354Gln mutant.

The C-terminal carboxylate of D1-Ala344 has been shown to provide peaks at 1356 cm^{-1} in the S_1 state and 1338 or 1320 cm^{-1} in the S_2 state by [1-^{13}C]Ala substitution and site-directed mutants of D1-Ala344 (*25*, *29*−*31*). It was later suggested that the 1338 cm^{-1} peak is a more likely candidate for the band in the S_2 state (*25*, *32*). Indeed, there are weak peaks at ~1340 cm^{-1} in both parallel and perpendicular polarizations, whereas almost no intensity was detected at 1320 cm^{-1} (Figure 4A). Thus, the band at 1340 cm^{-1} is expected to have a large contribution from the C-terminal carboxylate in the S_2 state. This band provided an angle of $47 \pm 4°$ (Table 1). On the other hand, the negative dip at 1352 cm^{-1} (Figure 4A) probably corresponds to the band of the C-terminal carboxylate in the S_1 state. Unfortunately, the overlap with a strong positive band at 1363 cm^{-1} hampers a proper estimation of the dichroic ratio of this dip. The X-ray structures have shown the orientation of the Ala344 carboxylate to be 73−81° (Table 2). The large difference in angles between FTIR and XRD could suggest a large orientation change in the C-terminal carboxylate upon the $S_1 \rightarrow S_2$ transition. However, alternative possibilities are that the 1340 cm^{-1} band is significantly overlapped by other vibrations with nearly perpendicular orientations and that the S_2 band is actually located at ~1320 cm^{-1} but the intensity is cancelled by the overlap of another negative band. It is also possible that the orientation of the C-terminus in the

X-ray structure is significantly changed from that in the intact OEC by X-ray damage to the Mn cluster.

The prominent negative band at 1401 cm^{-1} and the positive band at 1363 cm^{-1} in the S_2/S_1 difference spectra (Figure 4A) have been shown to disappear upon depletion of Ca^{2+} (*26*, *55*) and thus have been proposed to arise from an identical carboxylate ligand in the S_1 and S_2 states, respectively. The 1363 cm^{-1} band is also known to be upshifted by NH_3 treatment (*56*). It has been proposed that this carboxylate ligand takes a bridging bidentate coordination in the S_1 state and a unidentate coordination in the S_2 state from the change in the frequency gap between asymmetric and symmetric COO^- vibrations (*26*). In spite of the clearest feature in the S_2/S_1 spectrum, the assignment of these bands to a specific carboxylate group has not been successful yet. The orientation of this carboxylate was estimated to be 45 ± 2° and 35 ± 3° in the S_1 and S_2 states, respectively (Table 1). The orientation change of ~10° is consistent with the coordination change from bidentate to unidentate structure during the $S_1 \rightarrow S_2$ transition, because in unidentate coordination, the orientation of the transition dipole of the "symmetric" COO^- vibration is slightly deviated to the side of the metal ion (*54*). The value of 45 ± 2° in the S_1 state is in the range of 43−74°, 15−62°, and 47−78° for D1-Glu333, D1-Asp342, and D1-Glu189, respectively, obtained by the X-ray structures (Table 2). No FTIR spectra of site-directed mutants of D1-Glu333 have been reported, while Strickler et al. (*57*, *58*) reported that mutations of D1-Asp342 and D1-Glu189 did not alter the symmetric COO^- bands in FTIR spectra upon $S_0 \rightarrow S_1$, $S_1 \rightarrow S_2$, and $S_2 \rightarrow S_3$ transitions. Therefore, D1-Glu333 is a possible candidate for these FTIR bands. In most of the OEC models determined by XRD studies (*7*, *8*) and by polarized EXAFS (*14*−*16*), D1-Glu333 coordinates two Mn ions, being consistent with the bridging bidentate coordination proposed by FTIR (*26*). However, D1-Glu333 is located away from Ca^{2+} in these models, which is inconsistent with the experimental observations that the 1401 and 1363 cm^{-1} bands are sensitive to Ca^{2+} depletion and thus should be strongly coupled to Ca^{2+}. Further mutational studies are necessary for the definite assignments of these prominent FTIR bands at 1401 and 1363 cm^{-1}.

The negative band at 1419 cm^{-1} and the positive band at 1435 cm^{-1} provide angles of 48 ± 3° and 34 ± 4°, respectively (Table 1). The relatively high frequencies of these bands in the symmetric COO^- region indicate that the corresponding carboxylate groups likely have chelating or bridging bidentate coordination (*54*, *59*, *60*). The candidates for the assignment of the 1419 cm^{-1} peak is the same as that for the 1401 and 1363 cm^{-1} peaks, i.e., D1-Glu333, D1-Asp342, and D1-Glu189. D1-Asp342 and D1-Glu189, however, do not contribute to the S_2/S_1 difference spectra as described above. Another candidate is D1-Asp61, which is not a direct ligand to the Mn cluster but is located near the Mn cluster and coupled with it through a hydrogen bond network (*6*−*9*). The orientation of D1-Asp61 in the X-ray structures ranges between 47° and 60° (Table 2), which is in agreement with the angle of 48 ± 3° for the 1419 cm^{-1} band. D1-Asp61 has been proposed to function as a mediator of proton transfer from the OEC to the lumenal side (*6*, *61*−*63*).

In conclusion, this study shows that light-induced polarized ATR-FTIR difference spectroscopy is a fruitful method for investigating the orientations of cofactors and the coupled amino acid side chains in photosynthetic membrane proteins. In particular, this method is useful for the study of orientations of the amino acid ligands to the metal center that is prone to X-ray damage, such as the Mn cluster. In the XRD studies, only the structure of the dark stable state (S_1 or more reduced states) has been detected (*6*−*9*). In contrast, this polarized ATR-FTIR study could produce the information of orientation changes in the carboxylate groups upon the $S_1 \rightarrow S_2$ transition. Polarized ATR-FTIR measurements of the S-state cycle via application of successive flashes would provide further information about the orientation changes of amino acids during the water oxidation reaction. Also, combinations of this method with site-directed mutagenesis, selective amino acid isotope labeling, and various chemical perturbations (e.g., Ca^{2+} depletion and metal substitution) will provide more accurate and specific information about the structure of individual ligands or amino acid residues involved in OEC reactions. The improvement in the resolution of X-ray structures in the near future will help more accurate assignments of the polarized FTIR bands, which will significantly contribute to unraveling the molecular mechanism of photosynthetic oxygen evolution.

ACKNOWLEDGMENT

We thank Mr. Ryouta Takahashi for the technical support for DFT calculations.

SUPPORTING INFORMATION AVAILABLE

Optimized geometry of the PQ-1 radical anion by DFT calculations with the direction of the transition dipole moment of the CO stretching vibration. This material is available free of charge via the Internet at http://pubs.acs.org.

REFERENCES

1. Debus, R. J. (1992) The manganese and calcium ions of photosynthetic oxygen evolution. *Biochim. Biophys. Acta 1102*, 269–352.
2. Hillier, W., and Messinger, J. (2005) Mechanism of photosynthetic oxygen production. In Photosystem II: The Light-Driven Water: Plastoquinone Oxidoreductase (Wydrzynski, T., and Satoh, K., Eds.) pp 567−608, Springer, Dordrecht, The Netherlands.
3. McEvoy, J. P., and Brudvig, G. W. (2006) Water-splitting chemistry of photosystem II. *Chem. Rev. 106*, 4455–4483.
4. Renger, G. (2007) Oxidative photosynthetic water splitting: Energetics, kinetics and mechanism. *Photosynth. Res. 92*, 407–425.
5. Renger, G., and Holzwarth, A. R. (2005) Primary electron transfer. In Photosystem II: The Light-Driven Water:Plastoquinone Oxidoreductase (Wydrzynski, T., and Satoh, K., Eds.) pp 139−175, Springer, Dordrecht, The Netherlands.
6. Ferreira, K. N., Iverson, T. M., Maghlaoui, K., Barber, J., and Iwata, S. (2004) Architecture of the photosynthetic oxygen-evolving center. *Science 303*, 1831–1838.
7. Loll, B., Broser, M., Kos, P. B., Kern, J., Biesiadka, J., Vass, I., Saenger, W., and Zouni, A. (2008) Modeling of variant copies of subunit D1 in the structure of photosystem II from *Thermosynechococcus elongatus*. *Biol. Chem. 389*, 609–617.
8. Guskov, A., Kern, J., Gabdulkhakov, A., Broser, M., Zouni, A., and Saenger, W. (2009) Cyanobacterial photosystem II at 2.9-Å resolution and the role of quinones, lipids, channels and chloride. *Nat. Struct. Mol. Biol. 16*, 334–342.
9. Kawakami, K., Umena, Y., Kamiya, N., and Shen, J.-R. (2009) Location of chloride and its possible functions in oxygen-evolving photosystem II revealed by X-ray crystallography. *Proc. Natl. Acad. Sci. U.S.A. 106*, 8567–8572.
10. Peloquin, J. M., Campbell, K. A., Randall, D. W., Evanchik, M. A., Pecoraro, V. L., Armstrong, W. H., and Britt, R. D. (2000) ^{55}Mn ENDOR of the S_2-state multiline EPR signal of photosystem II: Implications on the structure of the tetranuclear Mn cluster. *J. Am. Chem. Soc. 122*, 10926–10942.
11. Hasegawa, K., Ono, T., Inoue, Y., and Kusunoki, M. (1999) Spin-exchange interactions in the S_2-state manganese tetramer in photosynthetic oxygen-evolving complex deduced from g = 2 multiline EPR signal. *Chem. Phys. Lett. 300*, 9–19.

12. Yano, J., Kern, J., Irrgang, K. D., Latimer, M. J., Bergmann, U., Glatzel, P., Pushkar, Y., Biesiadka, J., Loll, B., Sauer, K., Messinger, J., Zouni, A., and Yachandra, V. K. (2005) X-ray damage to the Mn_4Ca complex in single crystals of photosystem II: A case study for metalloprotein crystallography. *Proc. Natl. Acad. Sci. U.S.A. 102*, 12047–12052.
13. Grabolle, M., Haumann, M., Muller, C., Liebisch, P., and Dau, H. (2006) Rapid loss of structural motifs in the manganese complex of oxygenic photosynthesis by X-ray irradiation at 10−300 K. *J. Biol. Chem. 281*, 4580–4588.
14. Yano, J., Kern, J., Sauer, K., Latimer, M. J., Pushkar, Y., Biesiadka, J., Loll, B., Saenger, W., Messinger, J., Zouni, A., and Yachandra, V. K. (2006) Where water is oxidized to dioxygen: Structure of the photosynthetic Mn_4Ca cluster. *Science 314*, 821–825.
15. Barber, J., and Murray, J. W. (2008) Revealing the structure of the Mn-cluster of photosystem II by X-ray crystallography. *Coord. Chem. Rev. 252*, 233–243.
16. Barber, J., and Murray, J. W. (2008) The structure of the Mn_4Ca^{2+} cluster of photosystem II and its protein environment as revealed by X-ray crystallography. *Philos. Trans. R. Soc. London, Ser. B 363*, 1129–1137.
17. Siegbahn, P. E. M. (2008) A structure-consistent mechanism for dioxygen formation in photosystem II. *Chem.—Eur. J. 14*, 8290–8302.
18. Zein, S., Kulik, L. V., Yano, J., Kern, J., Pushkar, Y., Zouni, A., Yachandra, V. K., Lubitz, W., Neese, F., and Messinger, J. (2008) Focusing the view on nature's water-splitting catalyst. *Philos. Trans. R. Soc. London, Ser. B 363*, 1167–1177.
19. Sproviero, E. M., Gascon, J. A., McEvoy, J. P., Brudvig, G. W., and Batista, V. S. (2008) A model of the oxygen-evolving center of photosystem II predicted by structural refinement based on EXAFS simulations. *J. Am. Chem. Soc. 130*, 6728–6730.
20. Noguchi, T., and Berthomieu, C. (2005) Molecular analysis by vibrational spectroscopy. In Photosystem II: The Light-Driven Water:Plastoquinone Oxidoreductase (Wydrzynski, T., and Satoh, K., Eds.) pp 367−387, Springer, Dordrecht, The Netherlands.
21. Berthomieu, C., and Hienerwadel, R. (2009) Fourier transform infrared (FTIR) spectroscopy. *Photosynth. Res. 101*, 157–170.
22. Chu, H.-A., Hillier, W., Law, N. A., and Babcock, G. T. (2001) Vibrational spectroscopy of the oxygen-evolving complex and of manganese model compounds. *Biochim. Biophys. Acta 1503*, 69–82.
23. Noguchi, T. (2007) Light-induced FTIR difference spectroscopy as a powerful tool toward understanding the molecular mechanism of photosynthetic oxygen evolution. *Photosynth. Res. 91*, 59–69.
24. Noguchi, T. (2008) Fourier transform infrared analysis of the photosynthetic oxygen-evolving center. *Coord. Chem. Rev. 252*, 336–346.
25. Debus, R. J. (2008) Protein ligation of the photosynthetic oxygen-evolving center. *Coord. Chem. Rev. 252*, 244–258.
26. Noguchi, T., Ono, T., and Inoue, Y. (1995) Direct detection of a carboxylate bridge between Mn and Ca^{2+} in the photosynthetic oxygen-evolving center by means of Fourier transform infrared spectroscopy. *Biochim. Biophys. Acta 1228*, 189–200.
27. Noguchi, T., and Sugiura, M. (2003) Analysis of flash-induced FTIR difference spectra of the S-state cycle in the photosynthetic water-oxidizing complex by uniform ^{15}N and ^{13}C isotope labeling. *Biochemistry 42*, 6035–6042.
28. Kimura, Y., Mizusawa, N., Ishii, A., Yamanari, T., and Ono, T. (2003) Changes of low-frequency vibrational modes induced by universal ^{15}N- and ^{13}C-isotope labeling in S_2/S_1 FTIR difference spectrum of oxygen-evolving complex. *Biochemistry 42*, 13170–13177.
29. Chu, H.-A., Hillier, W., and Debus, R. J. (2004) Evidence that the C-terminus of the D1 polypeptide of photosystem II is ligated to the manganese ion that undergoes oxidation during the S_1 to S_2 transition: An isotope-edited FTIR study. *Biochemistry 43*, 3152–3166.
30. Strickler, M. A., Walker, L. M., Hillier, W., and Debus, R. J. (2005) Evidence from biosynthetically incorporated strontium and FTIR difference spectroscopy that the C-terminus of the D1 polypeptide of photosystem II does not ligate calcium. *Biochemistry 44*, 8571–8577.
31. Kimura, Y., Mizusawa, N., Yamanari, T., Ishii, A., and Ono, T. (2005) Structural changes of D1 C-terminal α-carboxylate during S-state cycling in photosynthetic oxygen evolution. *J. Biol. Chem. 280*, 2078–2083.
32. Strickler, M. A., Hwang, H. J., Burnap, R. L., Yano, J., Walker, L. M., Service, R. J., Britt, R. D., Hillier, W., and Debus, R. J. (2008) Glutamate-354 of the CP43 polypeptide interacts with the oxygen-evolving Mn_4Ca cluster of photosystem II: A preliminary characterization of the Glu354Gln mutant. *Philos. Trans. R. Soc. London, Ser. B 363*, 1179–1187.
33. Shimada, Y., Suzuki, H., Tsuchiya, T., Tomo, T., Noguchi, T., and Mimuro, M. (2009) Effect of a single amino acid substitution of the 43 kDa chlorophyll-protein on the oxygen-evolving reaction of the cyanobacterium *Synechocystis* sp. PCC 6803: Analysis of the Glu354Gln mutation. *Biochemistry 48*, 6095–6103.
34. Noguchi, T., Inoue, Y., and Tang, X.-S. (1999) Structure of a histidine ligand in the photosynthetic oxygen-evolving complex as studied by light-induced Fourier transform infrared difference spectroscopy. *Biochemistry 38*, 10187–10195.
35. Kimura, Y., Mizusawa, N., Ishii, A., and Ono, T. (2005) FTIR detection of structural changes in a histidine ligand during S-state cycling of photosynthetic oxygen-evolving complex. *Biochemistry 44*, 16072–16078.
36. Tang, X.-S., Diner, B. A., Larsen, B. S., Gilchrist, M. L., Lorigan, G. A., and Britt, R. D. (1994) Identification of histidine at the catalytic site of the photosynthetic oxygen-evolving complex. *Proc. Natl. Acad. Sci. U.S.A. 91*, 704–708.
37. Goormaghtigh, E., Raussens, V., and Ruysschaert, J. M. (1999) Attenuated total reflection infrared spectroscopy of proteins and lipids in biological membranes. *Biochim. Biophys. Acta 1422*, 105–185.
38. Arkin, I. T., Rothman, M., Ludlam, C. F., Aimoto, S., Engelman, D. M., Rothschild, K. J., and Smith, S. O. (1995) Structural model of the phospholamban ion channel complex in phospholipid membranes. *J. Mol. Biol. 248*, 824–834.
39. Rodionova, N. A., Tatulian, S. A., Surrey, T., Jähnig, F., and Tamm, L. K. (1995) Characterization of two membrane-bound forms of OmpA. *Biochemistry 34*, 1921–1929.
40. Ding, F. X., Xie, H. B., Arshava, B., Becker, J. M., and Naider, F. (2001) ATR-FTIR study of the structure and orientation of transmembrane domains of the *Saccharomyces cerevisiae* α-mating factor receptor in phospholipids. *Biochemistry 40*, 8945–8954.
41. Martin, I., Goormaghtigh, E., and Ruysschaert, J.-M. (2003) Attenuated total reflection IR spectroscopy as a tool to investigate the orientation and tertiary structure changes in fusion proteins. *Biochim. Biophys. Acta 1614*, 97–103.
42. Iwaki, M., Andrianambinintsoa, S., Rich, P., and Breton, J. (2002) Attenuated total reflection Fourier transform infrared spectroscopy of redox transitions in photosynthetic reaction centers: Comparison of perfusion- and light-induced difference spectra. *Spectrochim. Acta, Part A 58*, 1523–1533.
43. Okubo, T., and Noguchi, T. (2007) Selective detection of the structural changes upon photoreactions of several redox cofactors in photosystem II by means of light-induced ATR-FTIR difference spectroscopy. *Spectrochim. Acta, Part A 66*, 863–868.
44. Ono, T., and Inoue, Y. (1986) Effects of removal and reconstitution of the extrinsic 33, 24 and 16 kDa proteins on flash oxygen yield in photosystem II particles. *Biochim. Biophys. Acta 850*, 380–389.
45. Rothschild, K. J., and Clark, N. A. (1979) Polarized infrared spectroscopy of oriented purple membrane. *Biophys. J. 25*, 473–488.
46. Nabedryk, E., and Breton, J. (1981) Orientation of intrinsic proteins in photosynthetic membranes. Polarized infrared spectroscopy of chloroplasts and chromatophores. *Biochim. Biophys. Acta 635*, 515–524.
47. Frisch, M. J., Trucks, G. W., Schlegel, H. B., Scuseria, G. E., Robb, M. A., Cheeseman, J. R., Montgomery, J. A., Jr., Vreven, T., Kudin, K. N., Burant, J. C., Millam, J. M., Iyengar, S. S., Tomasi, J., Barone, V., Mennucci, B., Cossi, M., Scalmani, G., Rega, N., Petersson, G. A., Nakatsuji, H., Hada, M., Ehara, M., Toyota, K., Fukuda, R., Hasegawa, J., Ishida, M., Nakajima, T., Honda, Y., Kitao, O., Nakai, H., Klene, M., Li, X., Knox, J. E., Hratchian, H. P., Cross, J. B., Bakken, V., Adamo, C., Jaramillo, J., Gomperts, R., Stratmann, R. E., Yazyev, O., Austin, A. J., Cammi, R., Pomelli, C., Ochterski, J. W., Ayala, P. Y., Morokuma, K., Voth, G. A., Salvador, P., Dannenberg, J. J., Zakrzewski, V. G., Dapprich, S., Daniels, A. D., Strain, M. C., Farkas, O., Malick, D. K., Rabuck, A. D., Raghavachari, K., Foresman, J. B., Ortiz, J. V., Cui, Q., Baboul, A. G., Clifford, S., Cioslowski, J., Stefanov, B. B., Liu, G., Liashenko, A., Piskorz, P., Komaromi, I., Martin, R. L., Fox, D. J., Keith, T., Al-Laham, M. A., Peng, C. Y., Nanayakkara, A., Challacombe, M., Gill, P. M. W., Johnson, B., Chen, W., Wong, M. W., Gonzalez, C., and Pople, J. A. (2004) Gaussian 03, revision C.02, Gaussian, Inc., Wallingford, CT.
48. Becke, A. D. (1993) Density-functional thermochemistry. III. The role of exact exchange. *J. Chem. Phys. 98*, 5648–5652.
49. Lee, C., Yang, W., and Parr, R. G. (1988) Development of the Colle-Salvetti correlation-energy formula into a functional of the electron density. *Phys. Rev. B 37*, 785–789.
50. Takano, A., Takahashi, R., Suzuki, H., and Noguchi, T. (2008) Herbicide effect on the hydrogen-bonding interaction of the primary quinone electron acceptor Q_A in photosystem II as studied by Fourier transform infrared spectroscopy. *Photosynth. Res. 98*, 159–167.

51. Berthomieu, C., Nabedryk, E., Mäntele, W., and Breton, J. (1990) Characterization by FTIR spectroscopy of the photoreduction of the primary quinone acceptor Q_A in photosystem II. *FEBS Lett. 269*, 363–367.
52. Pushkar, Y., Yano, J., Glatzel, P., Messinger, J., Lewis, A., Sauer, K., Bergmann, U., and Yachandra, V. (2007) Structure and orientation of the Mn_4Ca cluster in plant photosystem II membranes studied by polarized range-extended X-ray absorption spectroscopy. *J. Biol. Chem. 282*, 7198–7208.
53. Schiller, H., Dittmer, J., Iuzzolino, L., Dörner, W., Meyer-Klaucke, W., Solé, V. A., Nolting, H.-F., and Dau, H. (1998) Structure and orientation of the oxygen-evolving manganese complex of green algae and higher plants investigated by X-ray absorption linear dichroism spectroscopy on oriented photosystem II membrane particles. *Biochemistry 37*, 7340–7350.
54. Nara, M., Torii, H., and Tasumi, M. (1996) Correlation between the vibrational frequencies of the carboxylate group and the types of its coordination to a metal ion: An *ab initio* molecular orbital study. *J. Phys. Chem. 100*, 19812–19817.
55. Taguchi, Y., and Noguchi, T. (2007) Drastic changes in the ligand structure of the oxygen-evolving Mn cluster upon Ca^{2+} depletion as revealed by FTIR difference spectroscopy. *Biochim. Biophys. Acta 1767*, 535–540.
56. Chu, H.-A., Feng, Y.-W., Wang, C.-M., Chiang, K.-A., and Ke, S.-C. (2004) Ammonia-induced structural changes of the oxygen-evolving complex in photosystem II as revealed by light-induced FTIR difference spectroscopy. *Biochemistry 43*, 10877–10885.
57. Strickler, M. A., Hillier, W., and Debus, R. J. (2006) No evidence from FTIR difference spectroscopy that glutamate-189 of the D1 polypeptide ligates a manganese ion that undergoes oxidation during the S_0 to S_1, S_1 to S_2, or S_2 to S_3 transitions in photosystem II. *Biochemistry 45*, 8801–8811.
58. Strickler, M. A., Walker, L. M., Hillier, W., Britt, R. D., and Debus, R. J. (2007) No evidence from FTIR difference spectroscopy that aspartate-342 of the D1 polypeptide ligates a Mn ion that undergoes oxidation during the S_0 to S_1, S_1 to S_2, or S_2 to S_3 transitions in photosystem II. *Biochemistry 46*, 3151–3160.
59. Deacon, G. B., and Phillips, R. J. (1980) Relationships between the carbon-oxygen stretching frequencies of carboxylato complexes and the type of carboxylate coordination. *Coord. Chem. Rev. 33*, 227–250.
60. Nakamoto, K. (1997) Infrared and Raman Spectra of Inorganic and Coordination Compounds, 5th ed., Part B, pp 59−62, John Wiley & Sons, New York.
61. Murray, J. W., and Barber, J. (2007) Structural characteristics of channels and pathways in photosystem II including the identification of an oxygen channel. *J. Struct. Biol. 159*, 228–237.
62. Ishikita, H., Saenger, W., Loll, B., Biesiadka, J., and Knapp, E. W. (2006) Energetics of a possible proton exit pathway for water oxidation in photosystem II. *Biochemistry 45*, 2063–2071.
63. Sproviero, E. M., Gascon, J. A., McEvoy, J. P., Brudvig, G. W., and Batista, V. S. (2008) Quantum mechanics/molecular mechanics study of the catalytic cycle of water splitting in photosystem II. *J. Am. Chem. Soc. 130*, 3428–3442.